Study of separation force in constrained surface projection stereolithography

Yayue Pan, Haiyang He, Jie Xu and Alan Feinerman
Department of Mechanical and Industrial Engineering, University of Illinois at Chicago, Chicago, Illinois, USA

Abstract

Purpose – Recently, the constrained surface projection stereolithography (SL) technology is gaining wider attention and has been widely used in the 3D printing industry. In constrained surface projection SL systems, the separation of a newly cured layer from the constrained surface is a historical technical barrier. It greatly limits printable size, process reliability and print speed. Moreover, over-large separation force leads to adhesion failures in manufacturing processes, causing broken constrained surface and part defects. Against this background, this paper investigates the formation of separation forces and various factors that affect the separation process in constrained surface projection SL systems.

Design/methodology/approach – A bottom-up projection SL testbed, integrated with an *in-situ* separation force measurement unit, is developed for experimental study. Separation forces under various manufacturing process settings and constrained surface conditions are measured *in situ*. Additionally, physical models are constructed by considering the liquid resin filling process. Experiments are conducted to investigate influences of manufacturing process settings, constrained surface condition and print geometry on separation forces.

Findings – Separation forces increase linearly with the separation speed. The deformation and the oxygen inhibition layer near the constrained surface greatly reduce separation forces. The printing area, area/perimeter ratio and the degree of porousness of print geometries have a combined effect on determining separation forces.

Originality/value – This paper studied factors that influence separation force in constrained surface SL processes. Constrained surface conditions including oxygen inhibition layer thickness, deformation and oxygen permeation capability were investigated, and their influences on separation forces were revealed. Moreover, geometric factors of printing layers that are significant on determining separation forces have been identified and quantified. This study on separation forces provides a solid base for future work on adaptive control of constrained surface projection SL processes.

Keywords Bottom-up projection, Constrained surface stereolithography, Polydimethylsiloxane (PDMS) coating, Print geometry, Process control, Separation force

Paper type Research paper

1. Introduction

Additive manufacturing (AM) processes, also known as 3D printing, solid freeform fabrication and rapid prototyping/manufacturing, is a class of manufacturing technologies that make three-dimensional (3D) objects by accumulating materials, usually in a layer-by-layer way (Gibson *et al.*, 2010; Crawford, 1999; Jacobs, 1992; Pan *et al.*, 2012a, 2012b, 2012c, 2012d; Zhou and Chen, 2012; Chen, 2007). It can fabricate parts directly from computer-aided design models without part-specific tooling or fixtures. As a direct manufacturing approach, AM processes can cost-effectively fabricate truly complex 3D shapes that were previously impossible (Pan and Chen, 2015,; Pan *et al.*, 2012a, 2012b, 2012c, 2012d; Pan *et al.*, 2011; Yoon *et al.*, 2014; Chu *et al.*, 2008; Wang *et al.*, 2005).

Stereolithography (SL) is one of the most important AM technologies currently available and also the first commercialized AM technology. In the SL process, liquid photosensitive polymer is cured through the use of an irradiation light source such as a digital light processing (DLP) projector or a laser beam (Melchels *et al.*, 2010; Kruth *et al.*, 1998; Zhang *et al.*, 1999) which supplies the amount of energy that is needed to induce a curing reaction, forming a highly cross-linked polymer. Compared to other polymer AM techniques such as extrusion or jetting processes, SL produces parts with the highest accuracy and the best surface finish. There are two ways to cure liquid polymer in SL, free surface method and constrained surface method (Ikuta and Hirowatari, 1993). As illustrated in Figure 1, with a free surface method, the free surface of the liquid polymer is exposed to light and solidified, and then a new layer of liquid polymer is coated on the solidified surface by lowering the platform down (Pan *et al.*, 2012a, 2012b, 2012c, 2012d). With a constrained surface method, a thin layer of liquid photopolymer is constrained between the platform or part and the liquid vat. The light penetrates the transparent bottom surface and cures the liquid polymer. By moving the platform up, new liquid polymer fills into the gap and gets cured. A 3D part is then built by accumulating the cured resin.

The constrained surface method has several advantages over a free surface method:

- The container depth is independent of the part height. Thus, a shallow vat can be used to reduce the required volume of the liquid resin.

The current issue and full text archive of this journal is available on Emerald Insight at: **www.emeraldinsight.com/1355-2546.htm**

Rapid Prototyping Journal
23/2 (2017) 353–361

[DOI 10.1108/RPJ-12-2015-0188]

Received 5 December 2015
Revised 11 April 2016
Accepted 17 April 2016

Figure 1 Illustration of SL systems

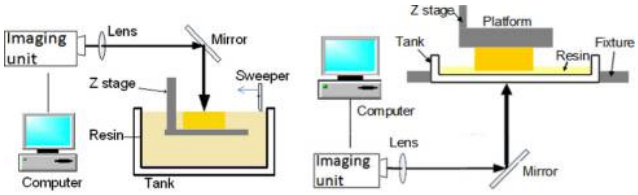

Notes: (Left) Free surface method; (Right) constrained surface method

- Much smaller layer thickness can be achieved because the gap size is only determined by the Z stage resolution, regardless of the fluid properties of liquid resin.
- A flat layer of a new liquid polymer could be refilled in a very short time, without any external assistance, and no matter how viscous the liquid is.

Such a constrained surface-based SL technology is gaining a lot of attention recently, and has been widely investigated and applied. For example, bottom-up projection SL is widely used in commercial SL machines from both established manufacturers such as 3D Systems and EnvisionTEC, and startup companies such as Formlabs and Carbon3D.

1.1 Separation challenge in constrained surface SL

Despite the advantages of the constrained surface SL process, a historical technical barrier, difficulty in separating a newly cured layer from the constrained surface, has never been completely solved and still significantly hinders the manufacturing capability and its applications. During the process of separating a newly cured layer from the bottom surface of the liquid vat, a separation force occurs. Such a separation force limits the printable size, manufacturing process reliability, print speed and life cycle of the constrained surface. Moreover, over-large separation force leads to many manufacturing defects and failures in SL, including holes in printed parts, adhesion of cured layers on constrained surface, separate layers, failed parts and broken constrained surface, as shown in Figure 2.

Attempts have been made to address this critical challenge of separation force. Non-sticky and air-permeable coatings, such as Teflon and polydimethylsiloxane (PDMS), are widely used to help the separation (Syao, 2014). Tumbleston *et al.* (2015) proposed to increase the oxygen inhibition layer thickness to decrease the separation force, by using highly air permeable coating or increasing oxygen concentration below

Figure 2 Manufacturing failures and defects caused by over-large separation force

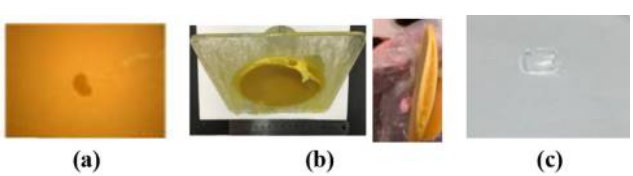

Notes: (a) Holes on printed surface; (b) separate layers; (c) broken film, which is functioning as the constrained surface

the constrained surface. In addition, Pan and Chen proposed a sliding mechanism to separate the part from the constrained surface (Pan *et al.*, 2012a, 2012b, 2012c, 2012d). Those approaches reduced separation forces greatly, compared to using a glass window. However, with an increase of printing area, separation force may still get too large, causing printing failures. In addition, separation force also limits the life cycle of coatings greatly. For example, a Teflon film or a PDMS film may be destroyed after a few prints.

Therefore, to improve manufacturing capability and avoid printing defects, it is critical to model separation forces. The force is determined by a combined effect of liquid polymer properties, print geometry (area and shape) and manufacturing system settings. Few research activities have been performed to investigate those factors quantitatively. Huang and Jiang (2005) identified that the pulling-up force is a function of the printing area and the moving velocity. The force is modeled by a pulling coefficient in their study. Liravi *et al.* (2012) proposed a cohesive delamination model to predict separation forces with different separation velocities. The effect of print geometries on separation force is still controversial. Huang and Jiang suggested that it has little effect, whereas Pan and Chen found that it does have some complicated effects on separation forces. Despite that pioneering work, effects of constrained surface condition have not been studied quantitatively yet, and how the manufacturing process and part geometry affect separation forces still remains largely unknown.

1.2 Contributions

Against the above background, a systematic separation force study is performed in this paper. A bottom-up projection SL setup is presented in Section 2. Separation forces are modeled in Section 3 and characterized experimentally in Section 4. Influences of the printing process and print geometries including separation speed, printing layer numbers, printing area, perimeters and porousness are modeled and measured using an *in-situ* force measurement method. Accordingly, approaches to eliminate the undesired influences by modifying the constrained surface conditions are presented in Section 5. Experimental comparisons verified the effectiveness of the proposed approach in controlling separation forces, elongating constrained surface life cycle and improving printing success rates.

2. Constrained surface stereolithography

2.1 Overview of the constrained surface SL

As discussed in Section 1, SL processes transform a prepolymer into a cross-linked polymer through a chain reaction initiated by free radicals or ions generated by light exposure, and stack cured polymer to make a 3D object, usually in a layer-by-layer fashion (Bártolo, 2011). Different light sources could be used, including visible radiation, UV radiation or infrared radiation. For all those different stereographic AM processes, separation force is a common challenge if the curing polymer is constrained by a surface.

In this paper, we investigate the separation force of a bottom-up projection-based SL, which is the mainstream of constrained surface SL systems now. A visible ultraviolet light with a bandwidth of 380-450 nm is used. A digital

micromirror device (DMD) is used to pattern the light to a digital mask. A DMD is a microelectromechanical system that enables one to simultaneously control approximately 1 million small mirrors that turn on or off a pixel at over 5 KHz. Using this technology, a light projection device can project a dynamically defined mask image onto a resin surface to selectively cure liquid resin into layers of the object. Besides, a conventional layer-by-layer accumulation mechanism is applied in this force study. The following section describes the experimental setup. Note that the force study findings could be applied to other constrained surface SL systems with different light sources and accumulation mechanisms.

2.2 Experimental setup

2.2.1 Hardware system

A bottom-up projection SL setup is built for the force study, as shown in Figure 3. It consists of an imaging unit, a resin vat which is an optically clear petri dish, a linear actuator that elevates the build platform, a controller and a load cell. The load cell is mounted directly on the build platform, so that real-time elevation force can be measured and recorded. In our setup, to assist the separation process, the bottom surface of the liquid vat is coated with PDMS. An off-the-shelf projector was used as the imagining unit. The optical lenses of the projector were modified to reduce the projection distance. Various projection settings, including focus, key stone rectification, brightness and contrast, were adjusted to achieve a sharp projection image on the designed projection plane. The DMD resolution in our system is 1,024 × 768 and the envelope size is set at 42.7 × 32 mm.

2.2.2 Software system

A digital mask planning testbed has been developed using the C++ language with Microsoft Visual Studio. The testbed integrates the geometry slicing and the motion controlling. It also synchronizes the image projection with Z movements. The graphical user-interface of the developed software system and flowchart of the manufacturing process are shown in Figure 3. In addition, an online force monitoring testbed has been developed in Matlab. It reads and processes data from the load cell, and records separation force measures in real time.

2.2.3 Materials

PerfactoryTM LS600M (yellow) from EnvisionTEC Inc. (Ferndale, MI) and G+ from MakerJuice Labs were used in experimental tests. Both resins belong to acrylate. For curing depths of 0.05 and 0.1 mm, the exposure time for LS600M and G+ based on our projection system are set at 45 and 2.8 s, respectively.

3. Influences of the manufacturing process on separation forces

3.1 Separation force modeling for solid circular geometry

In constrained surface SL processes, after the light irradiation, the Z stage moves up, separating the newly cured polymer from the constrained surface. Meanwhile, the liquid resin fills into the gap created during the separation process due to suction pressure. As shown in Figure 4(a), pulling-up force F, also called separation force, occurs during the process for a given separation velocity V. A is the cross-sectional size of the newly cured layer, and h is the height of the gap between the newly cured layer and the constrained surface. An analytical model was developed to predict the suction pressure and force while building an axisymmetric part. The model has the following assumptions: the part is a solid cylinder with a radius R, the bottom surface is rigid and the resin viscosity is constant and does not change over time.

Based on the Navier–Stokes equations (Bruus, 2008), the liquid flow velocity can be described in the following form:

$$u = \frac{1}{2\mu}\frac{dP}{dr}(Z^2 - Z \cdot h) \quad (1)$$

Figure 3 A bottom-up projection SL setup with *in-situ* separation force measuring

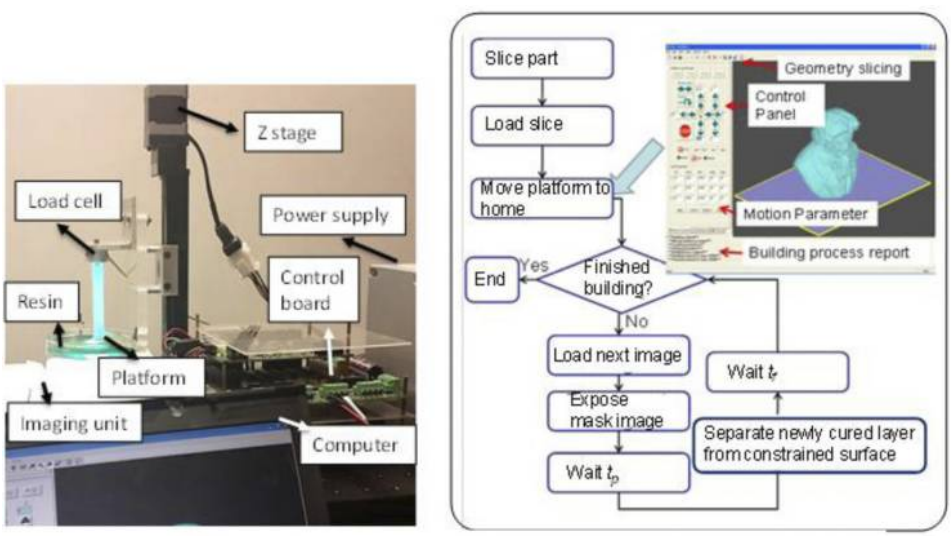

Notes: (a) Hardware setup; (b) flow chart and software setup

Figure 4 Schematic of separation forces for solid circular geometry

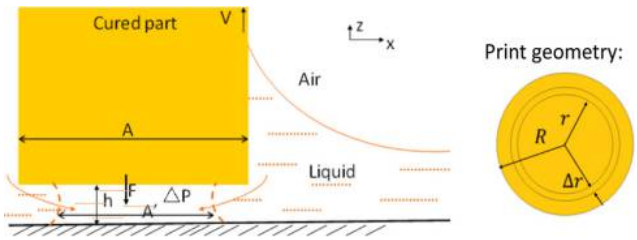

Then, according to the mass conservation equation, the relationship between the Z stage moving speed and liquid flow speed can be found as follows:

$$V \cdot \pi \cdot r^2 = 2 \cdot \pi \cdot r \int_0^h u dz \quad (2)$$

Substituting equation (1) into equation (2), we obtain the following:

$$V \cdot \mu \cdot r = \int_0^h \frac{\partial P}{\partial r} \cdot (Z^2 - Z \cdot h) dz \quad (3)$$

Integral both sides of equation (3) with respect to r, we can get:

$$P = -\frac{3\mu V}{h^3} \cdot r^2 + C \quad (4)$$

By applying the boundary condition that $r = R$, $P = 0$, the pressure is calculated to be:

$$P = -\frac{3\mu V}{h^3} \cdot r^2 + \frac{3\mu V}{h^3} \cdot R^2 \quad (5)$$

Accordingly, the pulling-up force can be acquired by integrating the pressure across the area:

$$F = \int_0^R 2\pi r P \, dr = \frac{3\pi \cdot \mu V}{2 \cdot h^3} \cdot R^4 \quad (6)$$

Note that the separation force F is nonlinear with R and h: $F \propto R^4$, $F \propto 1/h^3$. Additionally, the pressure and force are linear with the elevation speed V. Besides, the pressure in the center of the solid cross-section decreases with R^2. It was identified that a very thin oxygen-aided inhibition layer (2.5-20 μm) could be formed near the surface, which keeps the liquid resin from photo-polymerization. Such a oxygen-aided inhibition layer is also called as "dead zone" by some researchers (Tumbleston *et al.*, 2015). Because of the oxygen-aided inhibition, the initial value of h, which is the initial gap size between the bottom surface of the resin vat and the solidified layer, is the thickness of this oxygen-aided inhibition layer thickness. The initial value of h depends on the oxygen concentration near the constrained surface.

From the above physical model, it can be seen that the separation force is determined by factors including the material viscosity μ, the oxygen-aided inhibition layer thickness h, pull-up velocity V and printing geometry, which can be characterized by the radius R when it is a solid cylinder. Among those factors, V is a process parameter that can be controlled easily in the SL system; h is determined by the oxygen permeability of the constrained surface and therefore can be controlled by manipulating the constrained surface; and the resin viscosity μ and the printing geometry R are determined by the print task submitted by customers. Therefore, it is clear that the separation speed V and gap size h are the only two factors that we can manipulate to avoid the over-large separation force during a print task. According to the physical model, the separation force decreases with decreasing speed V and increasing gap size h. To verify this finding, experiments have been performed. Results are discussed in Sections 3.2 and 4.

3.2 Influence of separation speed on separation force

Experiments have been conducted to investigate the influence of separation speed, that is, z stage moving speed, on the separation force. Five separation speeds were tested: 0.63, 1.00, 1.56, 2.00 and 3.00 mm/s, with two different constrained surfaces: a glass surfaces coated with 2-mm-thick PDMS films, and a glass surfaces coated with 4-mm-thick PDMS films. A period of measured forces during building one layer with a 2-mm-thick PDMS surface is shown in Figure 5(a). Maximum separation forces for the speeds were calculated by taking an average of the measurements of replicated experiments. As plotted in Figure 5(b), the average of measured maximum forces for the 2-mm-thick PDMS surface are 0.72, 0.98, 1.18, 1.54 and 2.44 N for the five separation speeds, namely, 0.63, 1.00, 1.56, 2.00 and 3.00 mm/s, respectively. The average of measured maximum forces for the 4-mm-thick PDMS surface are 0.35, 0.50, 0.81, 1.01, and 1.40 N for the five separation speeds, respectively.

The experimental results verified the linear relationship modeled in Section 3.1, that is, the force peak increases with separation speeds with an approximated linear relationship. The identified relationship between separation force and pull-up separation speed is consistent with the findings in literature (Huang and Jiang, 2005). To further verify the role of gap size h in determining the separation force as found in our physical model, constrained surfaces have been modified and experiments have been performed, as discussed in following section.

4. Influences of constrained surface conditions on separation forces

The constrained surface that we focused on in this study is a PDMS film, which has a good elasticity and presents good oxygen inhibition capability (McCaig and Paul, 2000; Kudo *et al.*, 2006). Because of the elasticity, the PDMS film deforms during the separation process and moves together with the part with a smaller velocity. Hence, the separation velocity is actually a difference of the pull-up velocity of the part and the pull-up velocity of the PDMS film. Different PDMS deformation profiles lead to different separation speed and, therefore, separation force. In addition, the oxygen-aided

Figure 5 Measured forces with different speeds

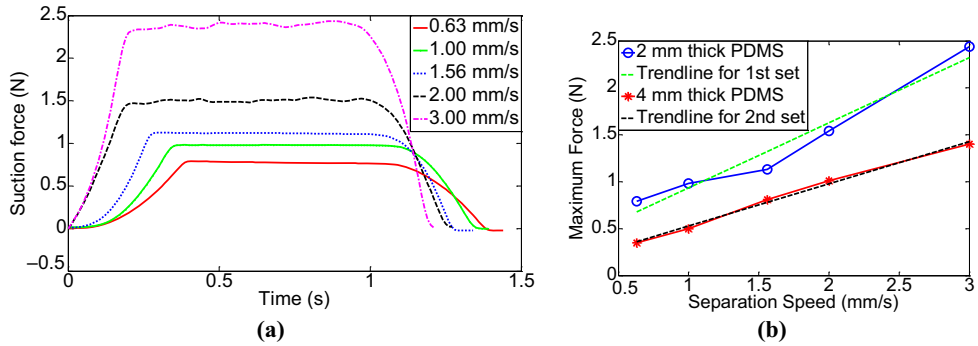

Notes: (a) An example of separation forces during building one layer with a 2-mm-thick PDMS surface and different speeds; (b) relationship between maximum separation force and separation speeds: Set 1 – force with a 2-mm-thick PDMS surface; Set 2 – force with a 4-mm-thick PDMS surface

inhibition layer thickness h varies with the thickness of the PDMS film and air permeability of the PDMS film (Firpo *et al.*, 2015). Therefore, by modifying the PDMS film, it is possible to adjust the separation speed V or the gap size h, to avoid over-large separation force. This section investigates influences of the thickness and oxygen permeability of PDMS film on separation forces experimentally.

4.1 Influence of PDMS thickness

Three sets of PDMS coatings, 1-mm-, 2-mm- and 4-mm-thick PDMS, were prepared. The Z-stage moving speed is fixed at 1.56 mm/s and the acceleration is 1.25 mm/s^2. Again, three replications were performed for each set of experiment. Figure 6 shows a period of measured separation forces for PDMS surfaces with thicknesses of 1, 2 and 4 mm. The average force peaks are measured to be 5.43, 1 and 0.73 N, respectively. The experimental results indicate that the maximum separation force decreases with the increase of the PDMS coating thickness. However, this trend of decreasing becomes less obvious if the PDMS thickness is bigger than 4 mm. This could be explained by a combined effect of its deformation and oxygen permeability. With the increase of PDMS film thickness, the oxygen permeability decreases slightly, and hence the inhibition layer thickness decreases (McCaig and Paul, 2000; Kudo *et al.*, 2006), leading to a slightly smaller h in equation (5) and hence a larger force in equation (6). On the other hand, the stiffness of the PDMS film decreases linearly with the increase of thickness (Daudeville *et al.*, 1995), leading to a larger deformation during a longer period. Because the PDMS deforms and moves up together with the printed part, the separation velocity V is actually the difference between the pull-up velocity of the part and the pull-up velocity of the PDMS film. With larger deformation of the PDMS film, the separation velocity V in equations (5) and (6) decreases, leading to a decreasing separation force. Because the oxygen permeability change is very slight for PDMS films with a thickness in the range of 1-2 mm, the PDMS film deformation plays a major role in this range, leading to a decreasing separation force, as shown in Figure 6.

Figure 6 Separation forces with various PDMS surfaces

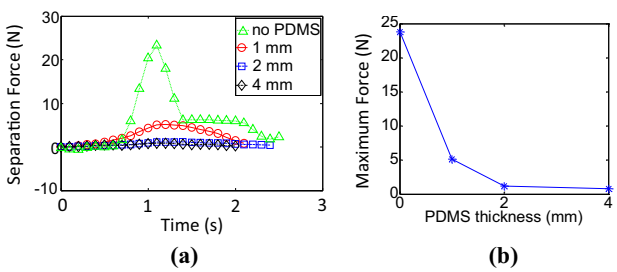

4.2 Influence of the oxygen inhibition layer thickness

It is also interesting to know whether the oxygen inhibition capability of the PDMS surface is stable during a long printing process. Experiments were conducted to record the separation force during the whole printing process of a 20-mm-tall object. As shown in Figure 7, as the printing process proceeds, separation forces increase from 2 N up to 20 N. This phenomenon could be explained by the consumption of oxygen near PDMS surfaces during the printing process, which makes the oxygen inhibition layer thickness h in equation (6) smaller. Therefore, for those parts that need a big number of layers, the separation force may get over-large in

Figure 7 Separation forces in the process of printing a 20 mm tall solid cylinder with conventional method (yellow curve) and new method (black curve)

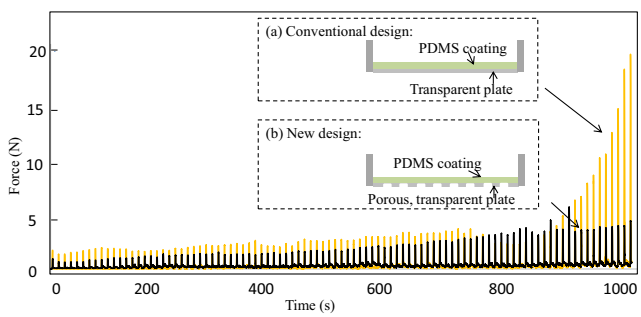

the process. It explains a common 3D printing failure, that is, layer adhesion failure occurs in the middle or at the end of the printing job.

Hence, to eliminate the undesired influence of the number of printed layers on separation forces, a sufficient and constant supply of oxygen is desired. Tumbleston *et al.* suggest that direct contact of air and oxygen permeable film could compensate the oxygen consumption in printing process, and therefore control separation forces (Chu *et al.*, 2008). Teflon AF 2400 was tested in their study and the feasibility has been verified. However, such a method introduces some other problems including tensioning challenge and creases of the film (Chu *et al.*, 2008). Because the PDMS-coated surface is another major type of constrained surface used in projection SL processes and no tensioning is required, this study focuses on the PDMS-coated surface only.

To address the increasing force problem, a new method of PDMS coating was developed and tested, as shown in Figure 7(b). The PDMS is coated on a porous transparent acrylic plate, which allows direct exposure of PDMS to the air. A 20-mm-tall solid cylinder was tested, with liquid vats that are coated with the conventional method [Figure 7(a)] and the new method [Figure 7(b)]. Measured separation forces with the two coating methods were plotted in Figure 7. With the conventional method, the separation force rises from 2 to 20 N in the printing process. With the new method, the separation force remains below 5 N during the whole printing process. The growing trend is effectively controlled with the new coating method.

5. Separation forces in printing complicated geometries

5.1 Irregular solid geometries

For irregular solid geometries as illustrated in Figure 8, the liquid velocity profile could be modified as:

$$u = \frac{1}{2\mu}\frac{dP}{d\lambda r(\theta)}(Z^2 - Z \cdot h) \tag{7}$$

where r is the radius at a certain angle θ, λ is an coefficient ranging from 0 to 1 and h is the gap distance between the bottom surface of the cured part and the constrained surface. By using the mass conservation equation, we could get:

Figure 8 Irregular solid cross section

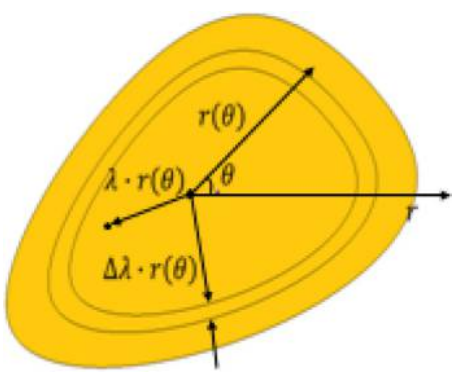

$$\lambda^2 \cdot V \cdot A = \lambda \cdot L \cdot \int_0^h u dz \tag{8}$$

where A is the area of the shape and L is the perimeter:

$$A = \int_0^{2\pi} \frac{1}{2} r(\theta)^2 d\theta \; ; \; L = \int_0^{2\pi} \theta \cdot r(\theta) d\theta \tag{9}$$

Substituting equation (7) into equation (8), we obtain the following:

$$2 \cdot \lambda \cdot \mu \cdot V \cdot A = L \cdot \int_0^h \frac{dP}{d\lambda r(\theta)}(Z^2 - Z \cdot h) dz \tag{10}$$

$$P = \frac{12 \cdot \mu \cdot V}{h^3} \cdot \frac{A}{L} \cdot \lambda^2 \cdot r(\theta) + C \tag{11}$$

By applying the boundary condition that $P(\lambda = 1) = 0$, the pressure and separation force can be obtained as follows:

$$\boldsymbol{P} = \frac{12 \cdot \boldsymbol{\mu} \cdot \boldsymbol{V}}{\boldsymbol{h}^3} \cdot \frac{\boldsymbol{A}}{\boldsymbol{L}} \cdot \boldsymbol{r}(\boldsymbol{\theta})(1 - \boldsymbol{\lambda}^2) \tag{12}$$

$$F = \frac{8 \cdot \mu \cdot V}{h^3} \cdot \frac{A}{L} \cdot \int_0^{2\pi} r(\theta) d\theta \tag{13}$$

Equations (12 and 13) indicate that, when the printing geometry is a solid shape, the separation force is a combined result of the material viscosity μ, gap size h, separation speed V and printing geometry. For irregular solid geometries, the influence of printing geometry on separation force could be modeled as a function of the area to perimeter ratio A/L and the radius r. Therefore, with fixed process parameters including h and V, and the same material, the same printing area with a smaller perimeter will bear larger separation force, and hence is more likely to cause manufacturing defects or failures. Therefore, with given materials and printing geometry, a larger gap size h or a smaller separation speed V are desired for layers with smaller perimeter.

To validate this, various solid geometries, including cylinder, hexagon, triangle and star, were tested. The print geometries of those structures are all solid cross-sections with an area of 314 mm^2. The area/perimeter ratios of those geometries range from 5 (cylinder structure) to 2.58 (star structure). Three replications were conducted for each test. Separation forces in the printing processes were measured. As shown in Figure 9, the maximum separation forces are found to be 6.16, 5.87, 5.45 and 4.9 N for cylinder, hexagon, triangle and star structures, respectively. The force peak increases linearly with the area/perimeter ratio of the print geometry, agreeing well with the analytical model in equation (13).

5.2 Porous geometries

For porous geometries, the influences of print geometry on separation forces become more complicated, as the liquid filling and constrained surface deformation are more complicated than the situation of printing solid geometries. Analytical modeling becomes very challenging. To explore the geometry influence, a group of hollowed geometries were

Figure 9 Separation forces for solid geometries with different area to perimeter ratio *A/L*

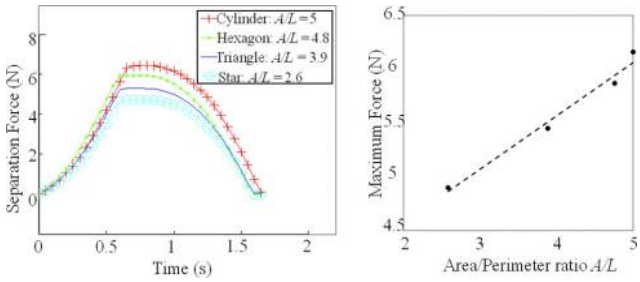

designed and tested. Figure 10 shows four print geometries with the same printing area, but different bounding box area. The porousness degree p is defined as the ratio of bounding box area to printing area. Hence, test a is a solid square that has a porousness degree of 1, whereas test d has the largest bounding box as well as the highest porousness ratio of 1.56.

Figure 11 shows the measured separation forces for the four test cases. It is shown that the separation force increases with the degree of porousness of the print geometry. This may be because of the extra pulling off effort for the porous area. Given the same printing area, a higher degree of porousness increases the "effective" separation area of the cured layer and hence increases the separation forces. However, the relationship between porousness degree and separation force is very complicated. It is also related to the shape of previous layers. If no deep holes are formed by the pervious layers in the porous areas of the current printing layer, the relationship could be approximated to be linear.

6. Discussion

As discussed in the introduction section, over-large separation force causes many manufacturing defects and failures,

Figure 10 Print geometries with various degrees of porousness

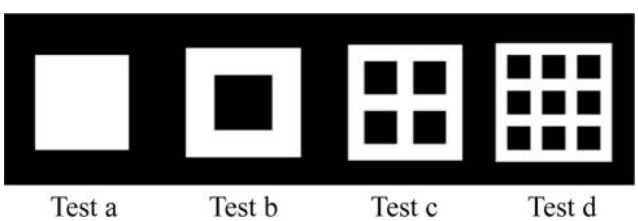

Figure 11 Separation forces for printing the four geometries in Figure 10

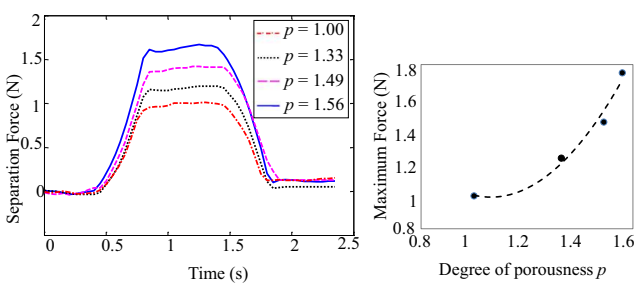

including holes in printed parts, separate layers and broken constrained surface. Therefore, it is critical to identify key parameters that dominate separation force and study the complicated relationship of process parameters, printing geometry and separation forces. Experimental results verified that the separation force increases with separation speeds, which agree with the literature. In addition, the separation force differs for different printing geometries, and it is changing during the printing process even with all process parameters fixed. Several new findings have been discovered in this study:

- Factors that influence separation force include initial oxygen-aided inhibition layer thickness h, pull-up speed V, material viscosity μ and printing geometry. Solid printing geometry and porous printing geometry affect the separation force in different ways.
- For solid geometries, the printing area to perimeter ratio A/L plays a significant role in determining separation forces. With the same printing area and process parameters, a geometry with a smaller perimeter will cause a larger separation force. The separation force increases linearly with the solid area to perimeter ratio A/L.
- For porous geometries, in addition to the printing area, porous areas of the printing layer also contribute to the increase of separation forces. With a fixed printing area, the separation force increases with the degree of porousness with an approximately polynomial relationship.
- Even with fixed process parameters and printing geometries, the separation force still may change dramatically during the printing process, causing the manufacturing process unreliable and unrepeatable. This is mainly because of the variation of the oxygen concentration near the constrained surface. When the oxygen supply is not enough, the thickness of the oxygen inhibition layer near the constrained surface is decreasing over the printing process, causing an increase in forces with the number of layers printed. Experimental results show that a porous air-permeable window is efficient in supplying oxygen consistently during the building process, providing an effective approach to control the increasing trend of separation force.

7. Conclusion

In this paper, the separation force in the constrained surface projection SL process has been investigated systematically. A testbed equipped with an *in-situ* force-monitoring unit has been developed. Relationships of separation forces with manufacturing process parameters, constrained surface conditions and print geometries have been explored experimentally and analytically. It is found that a faster separation speed will lead to larger separation force. Solid print geometries and porous geometries affect separation forces in different ways. Moreover, experimental results indicate that a porous constrained surface design with consistent air supplies is an effective approach to control the increasing trend of separation force in building process.

Some future work includes developing an adaptive process control methodology for predicting, and self-correcting forces

in constrained surface SL systems; and exploring constrained surface SL processes for large-area and high-throughput printing applications.

References

Bártolo, P.J. (Ed.). (2011), *Stereolithography: Materials, Processes and Applications*, Springer Science & Business Media, Berlin.

Bruus, H. (2008), *Theoretical Microfluidics*, Oxford University Press, Oxford.

Chen, Y. (2007), "3d texture mapping for rapid manufacturing", *Computer-Aided Design and Applications*, Vol. 4 No. 6, pp. 761-771.

Chu, C., Graf, G. and Rosen, D.W. (2008), "Design for additive manufacturing of cellular structures", *Computer-Aided Design and Applications*, Vol. 5 No. 5, pp. 686-696.

Crawford, R.H. (1999), "Solid freeform fabrication", *Spectrum, IEEE*, Vol. 36 No. 2, pp. 34-43.

Daudeville, L., Allix, O. and Ladevèze, P. (1995). "Delamination analysis by damage mechanics: some applications", *Composites Engineering*, Vol. 5 No. 1, pp. 17-24.

Firpo, G., Angeli, E., Repetto, L. and Valbusa, U. (2015). "Permeability thickness dependence of polydimethylsiloxane (PDMS) membranes", *Journal of Membrane Science*, Vol. 481, pp. 1-8.

Gibson, I., Rosen, D. and Stucke, B. (2010), *Additive Manufacturing Technologies*, Springer, New York, NY.

Huang, Y.M. and Jiang, C.P. (2005), "On-line force monitoring of platform ascending rapid prototyping system", *Journal of Materials Processing Technology*, Vol. 159 No. 2, pp. 257-264.

Ikuta, K. and Hirowatari, K. (1993), "Real three dimensional micro fabrication using stereo lithography and metal molding", *Micro Electro Mechanical Systems, 1993, MEMS'93, Proceedings An Investigation of Micro Structures, Sensors, Actuators, Machines and Systems*, IEEE, pp. 42-47.

Jacobs, P.F. (1992), *Rapid Prototyping & Manufacturing: Fundamentals of Stereolithography*, Society of Manufacturing Engineers, Dearborn, MI.

Kruth, J.P., Leu, M.C. and Nakagawa, T. (1998), "Progress in additive manufacturing and rapid prototyping", *CIRP Annals-Manufacturing Technology*, Vol. 47 No. 2, pp. 525-540.

Kudo, H., Sawadaa, T. Kazawab, E., Yoshidab, H., Iwasakic, Y., Mitsubayashi, K. (2006). "A flexible and wearable glucose sensor based on functional polymers with Soft-MEMS techniques", *Biosensors and Bioelectronics*, Vol. 22 No. 4, pp. 558-562.

Liravi, F., Zhou, C. and Das, S. (2014), "Separation force analysis based on cohesive delamination model for bottom-up stereolithography using finite element analysis", *Solid Freeform Fabrication Symposium*, Austin, TX, pp. 1432-1451.

McCaig, M.S. and Paul, D.R. (2000), "Effect of film thickness on the changes in gas permeability of a glassy polyarylate due to physical agingPart I. experimental observations", *Polymer*, Vol. 41 No. 2, pp. 629-637.

Melchels, F.P., Feijena, J., Grijpma, D.W. (2010), "A review on stereolithography and its applications in biomedical engineering", *Biomaterials*, Vol. 31 No. 24, pp. 6121-6130.

Pan, Y., Chen, Y. and Zhou, C. (2011), "Fabrication of smooth surfaces based on mask projection stereolithography", *Proceedings of the 22nd Solid Freeform Fabrication Symposium*, Austin, TX, p. 263-278.

Pan, Y., Zhou, C. and Chen, Y. (2012a), "A fast mask projection Stereolithography process for fabricating digital models in minutes", *Journal of Manufacturing Science and Engineering*, Vol. 134 No. 5, pp. 051011.

Pan, Y., Chen, Y. and Zhou, C. (2012b), "Fast recoating methods for the projection-based stereolithography process in micro- and macro-scales", *Proceedings of Solid Freeform Fabrication Symposium*, Austin, TX, pp. 846-862.

Pan, Y., Zhou, C. and Chen, Y. (2012c), "Rapid manufacturing in minutes: The development of a mask projection stereolithography process for high-speed fabrication", *ASME 2012 International Manufacturing Science and Engineering Conference collocated with the 40th North American Manufacturing Research Conference and in participation with the International Conference on Tribology Materials and Processing*, American Society of Mechanical Engineers, *Notre Dame*, pp. 405-414.

Pan, Y., Zhao, X. Zhou, C. and Chen, Y. (2012d), "Smooth surface fabrication in mask projection based stereolithography", *Journal of Manufacturing Processes*, Vol. 14 No. 4, pp. 460-470.

Pan, Y. and Chen, Y. (2013), "Fast micro-stereolithography process based on bottom-up projection for complex geometry", *Proceedings of the 8th International Conference on Micro Manufacturing, ICOMM 2013, Victoria*, pp. 1-8.

Pan, Y. and Chen, Y. (2015), "Smooth surface fabrication based on controlled meniscus and cure depth in micro-stereolithography", *ASME*, Vol. 3 No. 3, pp. 031001-031001-11.

Syao, K. (2014), "Stereolithography apparatus", U.S. Patent Application 14/454,901, filed August 8, 2014.

Tumbleston, J.R., Shirvanyants, D., Ermoshkin, N., Janusziewicz, R., Johnson, A.R., Kelly, D., Chen, K., Pinschmidt, R., Rolland, J.P., Ermoshkin, A., Samulski, E.T. and DeSimone, J.M. (2015), "Continuous liquid interface production of 3D objects", *Science*, Vol. 347 No. 6228, pp. 1349-1352.

Wang, H., Chen, Y. and Rosen, D.W. (2005), "A hybrid geometric modeling method for large scale conformal cellular structures", *ASME 2005 International Design Engineering Technical Conferences and Computers and Information in Engineering Conference, American Society of Mechanical Engineers, California*, pp. 421-427.

Yoon, J., He, D., Van Hecke, B. (2014), "A PHM approach to additive manufacturing equipment health monitoring, fault diagnosis, and quality control", *Annual Conference Of The Prognostics And Health Management Society, Fort Worth, TX*, pp. 1-9.

Zhang, X., Jiang, X.N. and Sun, C. (1999), "Micro-stereolithography of polymeric and ceramic microstructures", *Sensors and Actuators A: Physical*, Vol. 77 No. 2, pp. 149-156.

Zhou, C. and Chen, Y. (2012), "Additive manufacturing based on optimized mask video projection for improved accuracy and resolution", *Journal of Manufacturing Processes*, Vol. 14 No. 2, pp. 107-118.

Further reading

Wohlers, T. and Gornet, T. (2011), "History of additive manufacturing", *Wohlers Report*, p. 24.

Corresponding author

Yayue Pan can be contacted at: yayuepan@uic.edu